Mineralogical Magazine, June 2017, Vol. 81(3), pp. 499–513

New minerals with a modular structure derived from hatrurite from the pyrometamorphic rocks. Part III. Gazeevite, $BaCa_6(SiO_4)_2(SO_4)_2O$, from Israel and the Palestine Autonomy, South Levant, and from South Ossetia, Greater Caucasus

E. V. Galuskin[1,*], F. Gfeller[2], I. O. Galuskina[1], T. Armbruster[2], A. Krzątała[1], Y. Vapnik[3], J. Kusz[4], M. Dulski[5], M. Gardocki[1], A. G. Gurbanov[6,7] and P. Dzierżanowski[8]

[1] Faculty of Earth Sciences, Department of Geochemistry, Mineralogy and Petrography, University of Silesia, Będzińska 60, 41-200 Sosnowiec, Poland
[2] Mineralogical Crystallography, Institute of Geological Sciences, University of Bern, Freiestrasse 3, CH-3012 Bern, Switzerland
[3] Department of Geological and Environmental Sciences, Ben-Gurion University of the Negev, POB 653, Beer-Sheva 84105, Israel
[4] Institute of Physics, University of Silesia, Uniwersytecka 4, 40-007 Katowice, Poland
[5] Silesian Centre for Education and Interdisciplinary Research, Institute of Material Science, 75 Pułku Piechoty 1a, 41-500 Chorzow, Poland
[6] Institute of Geology of Ore Deposits, Petrography, Mineralogy and Geochemistry (IGEM), Russian Academy of Sciences, Staromonetny 35, 119017 Moscow, Russia
[7] Vladikavkaz Scientific Centre of the Russian Academy of Sciences, Markov str. 93a, 362008 Vladikavkaz, Republic of North Ossetia-Alania, Russia
[8] Institute of Geochemistry, Mineralogy and Petrology, Warsaw University, al. Żwirki i Wigury 93, 02-089 Warszawa, Poland

[*Received 13 February 2016; Accepted 29 March 2016; Associate Editor: G. Diego Gatta*]

ABSTRACT

The new mineral gazeevite, $BaCa_6(SiO_4)_2(SO_4)_2O$ ($R\bar{3}m$, $a = 7.1540(1)$, $c = 25.1242(5)$ Å, $V = 1113.58(3)$ Å^3, $Z = 3$), was found in an altered xenolith in rhyodacites of the Shadil-Khokh volcano, Southern Ossetia and at three localities in larnite pyrometamorphic rocks of the Hatrurim Complex; Nahal Darga and Jabel Harmun, Judean Mountains, Palestinian Autonomy, and Har Parsa, Negev Desert, Israel. Larnite, fluorellestadite–fluorapatite, srebrodolskite–brownmillerite and mayenite-supergroup minerals are the main minerals commonly associated with gazeevite. Gazeevite is isostructural with zadovite and aradite; the 1:1 type $AB_6(TO_4)_2(TO_4)_2W$, occurs together with the structurally related minerals of the nabimusaite series, 3:1 type $AB_{12}(TO_4)_4(TO_4)_2W_3$, where A = Ba, K, Sr…; B = Ca, Na…; T = Si, P, V^{5+}, S^{6+}, Al…; $W = O^{2-}$, F^-. Single antiperovskite layers $\{[WB_6](TO_4)_2\}$ in the structure type of gazeevite–zadovite and triple $\{[W_3B_{12}](TO_4)_4\}$ layers in arctite–nabimusaite are intercalated with single $A(TO_4)$ layers. These minerals with an interrupted antiperovskite structure are characterized by a modular layered structure derived from hatrurite, $Ca_3(SiO_4)O$. Gazeevite is colourless, transparent, with a white streak and vitreous lustre. Gazeevite is brittle, shows pronounced parting and imperfect cleavage on {001}; it is uniaxial (–), $\omega = 1.640(3)$, $\varepsilon = 1.636(2)$ ($\lambda = 589$ nm) and nonpleochroic; Mohs' hardness is ~4.5, $VHN_{50} = 417$ kg mm^{-2}. The calculated density

*E-mail: evgeny.galuskin@us.edu.pl
https://doi.org/10.1180/minmag.2016.080.105

is = 3.39 g cm^{-3}. The main lines of the calculated powder X-ray diffraction pattern are as follows (d(Å)/I/hkl): 3.58/100/110, 3.07/91/021, 2.76/47/116, 1.789/73/220, 3.29/60/113, 2.78/36/024, 2.12/25/125, 2.21/21/208. Raman spectra of gazeevite are compared with spectra of other minerals. The formation of gazeevite and minerals of the nabimusaite–dargaite series is connected with high-temperature alteration of an early assemblage of clinker minerals affected by later fluids generated by volcanic activity or combustion processes.

Keywords: gazeevite, new mineral, South Ossetia, Greater Caucasus, Palestine Autonomy, South Levant, hatrurite, modular structure.

Introduction

The new mineral gazeevite, $BaCa_6(SiO_4)_2(SO_4)_2O$ ($R\bar{3}m$, $a = 7.1540(1)$, $c = 25.1242(5)$ Å, $V = 1113.58(3)$ Å^3, $Z = 3$), was found in larnite rocks of the Hatrurim Complex (Israel, Palestinian Autonomy) and in an altered carbonate-silicate xenolith from a rhyodacite flow of the Shadil-Khokh volcano, Sothern Ossetia, Greater Caucasus. Gazeevite is isomorphous with zadovite and aradite (Table 1), which were discovered in thin paralava veins in gehlenite rocks of the Hatrurim Basin, Negev Desert, Israel (Galuskin *et al.*, 2015*a*). Gazeevite occurs together with the structurally related minerals of the nabimusaite–dargaite series (Table 1), forming a continuous solid solution (Galuskin *et al.*, 2015*b*). These minerals are characterized by a modular, layered structure derived from that of hatrurite, $Ca_3(SiO_4)O$. Hatrurite (cement name 'alite') exists in various polymorphic forms but all are strongly pseudo-rhombohedral ($R\bar{3}m$) with $a \approx 7.0$, $c \approx 25$ Å in the hexagonal setting (Jeffery, 1952; Nishi and Takéuchi, 1984; Mumme, 1995). The rhombohedral approximation of the 'alite' or hatrurite structure is sufficient to show the modular relation between $Ca_3(SiO_4)O$ and the newly described minerals gazeevite, nabimusaite, zadovite, aradite and dargaite.

The phosphate mineral arctite is isostructural with nabimusaite and dargaite (Table 1). Arctite and the synthetic phases (Table 1) $KCa_{12}(SiO_4)_4(SO_4)_2O_2F$ (Fayos *et al.*, 1985) and $Ca_{5.45}Li_{3.55}[SiO_4]_3O_{0.45}F_{1.55}$ (Krüger, 2010) are considered to have intercalated antiperovskite structures (Krivovichev, 2008; Krüger, 2010), for which octahedra are anion-centred and tetrahedra are cation-centred. The structure type of arctite–nabimusaite (3:1 type) is described by the common formula $AB_{12}(TO_4)_4(TO_4)_2W_3$, and that of gazeevite–zadovite (1:1 type) by $AB_6(TO_4)_2(TO_4)_2W$; where A = Ba, K, Sr …; B = Ca, Na; T = Si, P, V^{5+}, S^{6+}, Al …; $W = O^{2-}$, F^-. Antiperovskite $\{[WB_6](TO_4)_2\}$ layers in the zadovite type structure and triple $\{[W_3B_{12}](TO_4)_4\}$ layers in arctite–nabimusaite type intercalate with single $A(TO_4)$ layers (Gfeller *et al.*, 2013; Galuskin *et al.*, 2015*a*,*b*).

Gazeevite was named in honour of Dr Viktor Magalimovich Gazeev (born 1954), research staff member of the Institute of Geology of Ore Deposits, Petrography, Mineralogy and Geochemistry of the Russian Academy of Sciences (IGEM RAS), Moscow, and of the Vladikavkaz Scientific Centre of the Russian Academy of Sciences, Vladikavkaz, Republic of North Ossetia-Alania, Russia. He is the discoverer of unique xenoliths within the Upper Chegem Caldera (Gazeev *et al.*, 2006), where more than 20 new mineral species were discovered; their descriptions have been co-authored by him. The altered silicate-carbonate xenolith in which gazeevite was discovered, in rhyodacite lavas of the Shadil-Khokh volcano in Southern Ossetia, was also detected by him (Gazeev *et al.*, 2012).

Type materials were deposited in the mineralogical collections of the Museum of Natural History in Bern (Switzerland), Bernastrasse 5, CH-3005 Bern, catalogue number NMBE 43125 (holotype, author number JBB11a, Jabel Harmun) and the Fersman Mineralogical Museum, Leninskiy Prospekt 18/2, 115162 Moscow, Russia, catalogue numbers 4713/1 (co-type, author's no. U11, Shadil-Khokh), 4713/2 (co-type, author's no. DR5D, Nahal Darga), 4713/3 (holotype, author's no. JBB11a, Jabel Harmun) and 4713/4 (co-type, author's no. ZP4A, Har Parsa). The mineral and name were approved by the Commission on New Minerals, Nomenclature and Classification (CNMNC) of the International Mineralogical Association (IMA), IMA2015-037.

Occurrence, morphology and chemistry of gazeevite

Gazeevite was found at four localities: (1) in an altered carbonate-silicate xenolith (~2.5 m in diameter) enclosed in rhyodacite lava on the north-west slope of the Shadil-Khokh volcano (age ~ 30 ka; Gazeev *et al.*, 2012), Kel' volcanic area, Greater Caucasus Mountain Range, Southern Ossetia (42°32.5′ N 44°18′ E) and (2–4) in larnite nodules

https://doi.org/10.1180/minmag.2016.080.105 Published online by Cambridge University Press

TABLE 1. A comparison of gazeevite and its related mineral species and synthetic materials.

Mineral name	Ideal formula	Space group	*a* (Å)	*c* (Å)	*V* (Å^3)	*Z*	Reference
Gazeevite	$BaCa_6(SiO_4)_2(SO_4)_2O$	$R\bar{3}m$	7.1540(1)	25.1242(5)	1113.58(3)	3	Present study
Zadovite	$BaCa_6[(SiO_4)(PO_4)][(PO_4)_2F$	$R\bar{3}m$	7.09660(10)	25.7284(3)	1122.13(3)	3	Galuskin *et al.* (2015*a*)
Aradite	$BaCa_6[(SiO_4)(VO_4)][(VO_4)_2F$	$R\bar{3}m$	7.1300(1)	26.2033(9)	1153.63(6)	3	Galuskin *et al.* (2015*a*)
Nabimusaite	$KCa_{12}(SiO_4)_4(SO_4)_2O_2F$	$R\bar{3}m$	7.1905(4)	41.251(3)	1847.1(2)	3	Galuskin *et al.* (2015*b*)
Dargaite	$BaCa_{12}(SiO_4)_4(SO_4)_2O_3$	$R\bar{3}m$	7.1874(4)	41.292(3)	1847.32(19)	3	Gfeller *et al.* (2015*a*)
Hatrurite	$Ca_3(SiO_4)O$	$R\bar{3}m$	7.135(6)	25.586(15)	1128.031	9	Nishi and Takéuchi (1984)
Arctite	$BaCa_7Na_5(PO_4)_6F_3$	$R\bar{3}m$	7.094	41.320	1800.83	3	Sokolova *et al.* (1984)
Synthetic phase	$KCa_{12}(SiO_4)_4(SO_4)_2O_2F$	$R\bar{3}m$	7.197(5)	41.224(28)	1894.20	3	Fayos *et al.* (1985)
Synthetic phase	$Ca_{5.45}Li_{3.55}[SiO_4]_3O_{0.45}F_{1.55}$	$R\bar{3}m$	7.137	41.459	1828.86	6	Krüger (2010)

from pseudo-conglomerates of pyrometamorphic rocks of the Hatrurim Complex ('Mottled zone'; Bentor 1960; Gross 1977; Vapnik *et al.*, 2007, Galuskina *et al.*, 2014*a*) at Judean Mountains localities (Palestinian Autonomy). Details: (2) Nahal Darga (31°35′ N 35°22′ E) and (3) Jabel Harmun (31°46′ N 35°26′ E); and in the Negev Desert (Israel) on the west slope of (4) Har Parsa (31°13′ N 35°17′ E).

Crystal morphology and chemical composition of gazeevite and associated minerals were examined using optical microscopes and Philips XL30 ESEM/EDAX and Phenom XL analytical electron scanning microscopes (Faculty of Earth Sciences, University of Silesia, Poland). Chemical analyses of gazeevite were performed with CAMECA SX100 probe (Institute of Geochemistry, Mineralogy and Petrology, University of Warsaw, Poland) at 15 kV and 20 nA using the following lines and standards: Ba*Lα*, S*Kα* – baryte; P*Kα* – apatite; Ca*Kα* – wollastonite; Mg*Kα*, Si*Kα* – diopside; Al*Kα*, K*Kα* – orthoclase; Ti*Kα* – rutile; Na*Kα* – albite, Sr*Lα* – $SrTiO_3$, F*Kα* – fluorphlogopite.

Gazeevite was found in the Autumn of 2012 in a specimen from the Shadil-Khokh volcano (Fig. 1). This xenolith was detected in 2010 and preliminary mineral data were published in 2012 (Gazeev *et al.*, 2012). Gazeevite in the sample is concentrated on the boundary between merwinite and spurrite zones (Fig. 1). Srebrodolskite–brownmillerite, often as a segregation, and accessory and rare minerals, including spinel–magnesioferrite, baryte, lakargiite, kerimasite and periclase, are noted in both zones. In the spurrite zone, minerals of the fluorellestadite–'chlorellestadite', chlormayenite–chlorkyuygenite series, and secondary minerals ettringite–thaumasite, hydrocalumite and calcite are widespread; rarely is oldhamite preserved. Minerals of the gehlenite–akermanite and wadalite–chlormayenite series, rondorfite, monticellite, bredigite and larnite are characteristic of the merwinite zone. The host rocks are generally fractured. In cracks, rusinovite, eltyubyuite, cuspidine, ternesite, jasmundite and its chorine analogue known as artificial 'alinite' were identified. In other parts of the xenolith Ca-humites (kumtyubeite, fluorchegemite) and galuskinite were noted in spurrite zones (Galuskina *et al.*, 2015*a*). Gazeevite from Southern Ossetia is represented by xenomorphic metacrysts up to 30–50 μm in size, sometimes with hexagonal outline (Fig. 1*c*). In one case, gazeevite intergrown with dargaite (second find in the World) was detected (Fig. 1*d*). Gazeevite was analysed for the first time in rocks of the Hatrurim Complex associated with the new mineral vapnikite, Ca_3UO_6

https://doi.org/10.1180/minmag.2016.080.105 Published online by Cambridge University Press

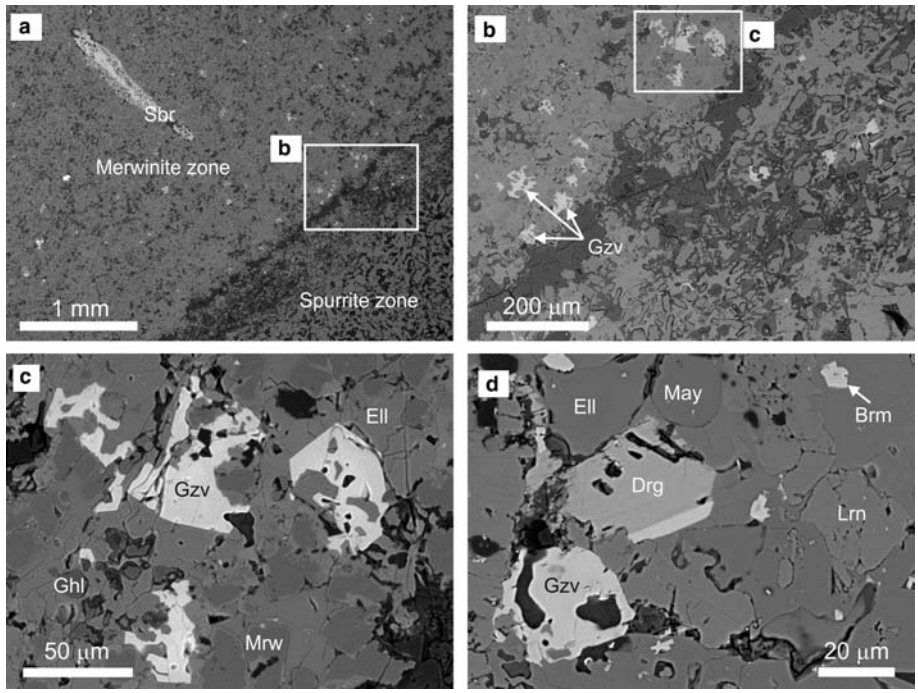

FIG. 1. Gazeevite from an altered xenolith in rhyodacites of the Shadil Khokh volcano, Southern Ossetia, back-scattered image (BSE). (*a*) General overview of the contact between merwinite and spurrite zones, elongated aggregates of srebrodolskite are characteristic for both zones. The framed area is magnified in Fig. 1*b*. (*b*) Gazeevite crystals concentrate at the contact area of the merwinite zone. The framed area is magnified in Fig. 1*c*. (*c*) Gazeevite metacrystals sometimes show a hexagonal outline. (*d*) Rarely gazeevite displays parallel growths with dargaite. Gzv = gazeevite, Ell = fluorellestadite, Ghl = gehlenite, Drg = dargaite, Mrw = merwinite, Lrn = larnite, Sbr = srebrodolskite, Brm = brownmillerite, May = chlormayenite.

(Galuskin *et al.*, 2014). All samples from this locality containing gazeevite are represented by larnite rocks. Larnite, brownmillerite, shulamitite, fluorellestadite–fluorapatite, fluormayenite–fluorkyuygenite, ye'elimite, gehlenite, ternesite, dargaite–nabimusaite, vapnikite, baryte, periclase and oldhamite are typical minerals in the rocks.

Data for gazeevite were obtained from all localities (Figs 1–3; Table 2). In general, physical properties were determined on different gazeevite grains from different localities. This became necessary due to the difficulty of extracting individual grains appropriate for various physical methods. All crystals used have very close chemical compositions. Compositions of type locality and co-type gazeevite from Southern Ossetia and larnite rocks of the Hatrurim Complex are similar. Nevertheless, gazeevite from larnite rocks of the Hatrurim Complex is slightly enriched in phosphorus (Table 2).

In the holotype specimen JBB11a from Jabel Harmun, grain aggregates of gazeevite (grains up to 40 μm) fill space between prismatic crystals of nabimusaite-dargaite (Fig. 2*a*). Structural data for gazeevite refer to this sample. Optical constants were measured on specimen DR5D (co-type) from Nahal Darga, in which gazeevite aggregates with spherulitic morphology and also fills spaces between nabimusiate crystals. Microhardness was measured on gazeevite from specimen ZP4A (co-type) of the Har Parsa locality. Here gazeevite forms xenomorphic poikiloblasts in porous fragments of larnite rocks with abundant larnite, ye'elimite and brownmillerite inclusions (Fig. 2*c*).

Gazeevite and nabimusaite are confined to larnite rock fragments of the Hatrurim Complex characterized by increasing porosity and/or the presence of visible microfractures. Investigation of the ZP4A specimen on a fresh surface showed that

https://doi.org/10.1180/minmag.2016.080.105 Published online by Cambridge University Press

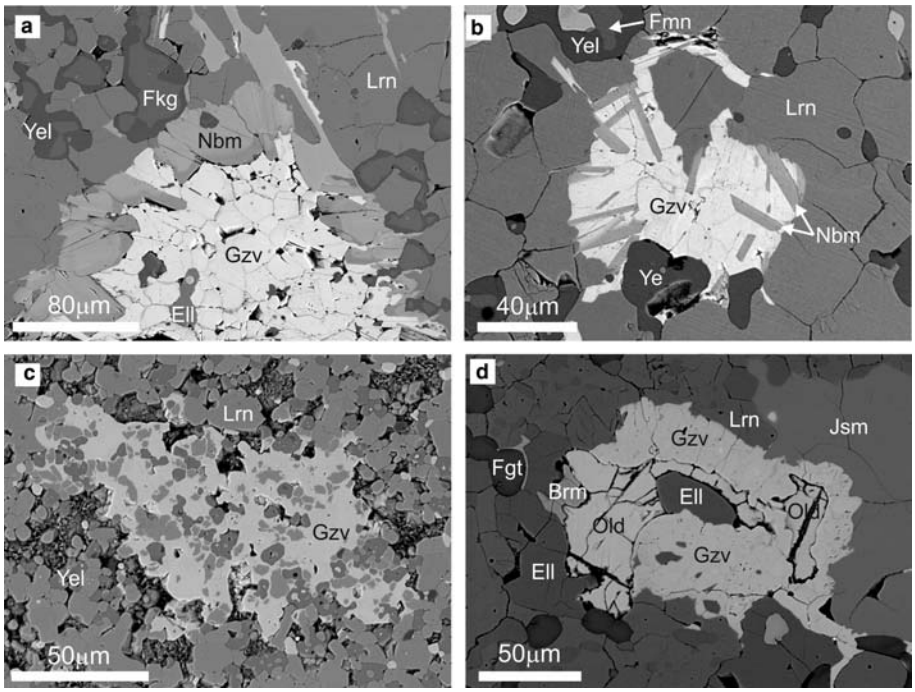

FIG. 2. Gazeevite in larnite rocks of the Hatrurim Complex, BSE. (*a*), (*b*) Grained aggregate of gazeevite filling space between nabimusaite crystals; (*a*) holotype specimen JJB11a; (*b*) co-type specimen DR5D. (*c*) Xenomorphic gazeevite in porous rock, co-type specimen ZP4A. (*d*) Gazeevite replacing oldhamite, Jabel Harmun. Gzv = gazeevite, Ell = fluorellestadite, Nbm = nabimusaite, Yel = ye'elimite, Jsm = jasmundite, Lrn = larnite, Fkg = fluorkyuygenite, Brm = brownmillerite, Fmn = fluormayenite, Old = oldhamite.

gazeevite is limited to a linear zone enriched in baryte, sylvite and calciolangbeinite (Fig. 3). Dissolution of the last two minerals is responsible for the porous texture of the microprobe mount studied (Fig. 2*c*). Other S-bearing minerals such as ternesite, rare jasmundite, appear in porous zones together with gazeevite and nabimusaite–dargaite (Galuskin *et al.*, 2015*a*,*b*; 2016). In these zones fluormayenite, $Ca_{12}Al_{14}O_{32}$ [$\square_4F_2$], transforms to fluorkyuygenite, $Ca_{12}Al_{14}O_{32}$ [$(H_2O)_4F_2$], if it is not shielded by a complete rim of ye'elimite (Fig. 2*a*, *b*, *d*). Nabimusaite–dargaite and gazeevite may replace fluorellestadite and, partially, larnite. In one case of a jasmundite-bearing rock, substitution of oldhamite by gazeevite is observed (Fig. 2*d*).

In pyrometamorphic rocks of the Hatrurim Complex a great number of new mineral species has been discovered during the last few years, in particular at localities characterized by the presence of gazeevite. Jabel Harmun is the type locality of harmunite, $CaFe_2O_4$ (Galuskina *et al.*, 2014*a*), nabimusaite (Galuskin *et al.*, 2015*b*), fluormayenite (Galuskin *et al.*, 2015*c*), vapnikite (Galuskin *et al.*, 2014) and dzierżanowskite $CaCu_2S_2$ (Galuskina *et al.*, 2014*b*). The area close to Nahal Darga is the type locality for dargaite (Gfeller *et al.*, 2015*a*). Mountain Parsa is within the largest outcrop of pyrometmorphic rocks of the Hatrurim Complex in Israel, and is known as the Hatrurim Basin. It is the type locality for barioferrite, $BaFe_{12}O_{19}$ (Murashko *et al.*, 2011), shulamitite, $Ca_3TiFeAlO_8$ (Sharygin *et al.*, 2013), negevite, NiP_2, halamishite, Ni_5P_4 and zuktamrurite, FeP_2 (Britvin *et al.*, 2015), zadovite and aradite (Galuskin *et al.*, 2015*a*), fluorkyuygenite (Galuskin *et al.*, 2015*c*), gurimite, $Ba_3(VO_4)_2$ (Galuskina *et al.*, 2013), flamite, $(Ca,Na,K)_2(Si,P)O_4$ (Sokol *et al.*, 2015; Gfeller *et al.*, 2015*b*), silicocarnotite, $Ca_5[(SiO_4)(PO_4)](PO_4)$ (Galuskin *et al.*, 2016), khesinite, $Ca_4(Mg_3Fe^{3+}_9)O_4(Fe^{3+}_9Si_3)O_{36}$ (Galuskina *et al.*, 2014*c*) and hexacelsian, $BaAl_2Si_2O_8$ (Galuskina *et al.*, 2015*b*).

Gazeevite is the first new mineral found in altered xenoliths of the Shadil-Khokh volcano; the second locality for kumtyubeite, fluorchegemite, rusinovite, dargaite and eltyubyuite (Galuskina

https://doi.org/10.1180/minmag.2016.080.105 Published online by Cambridge University Press

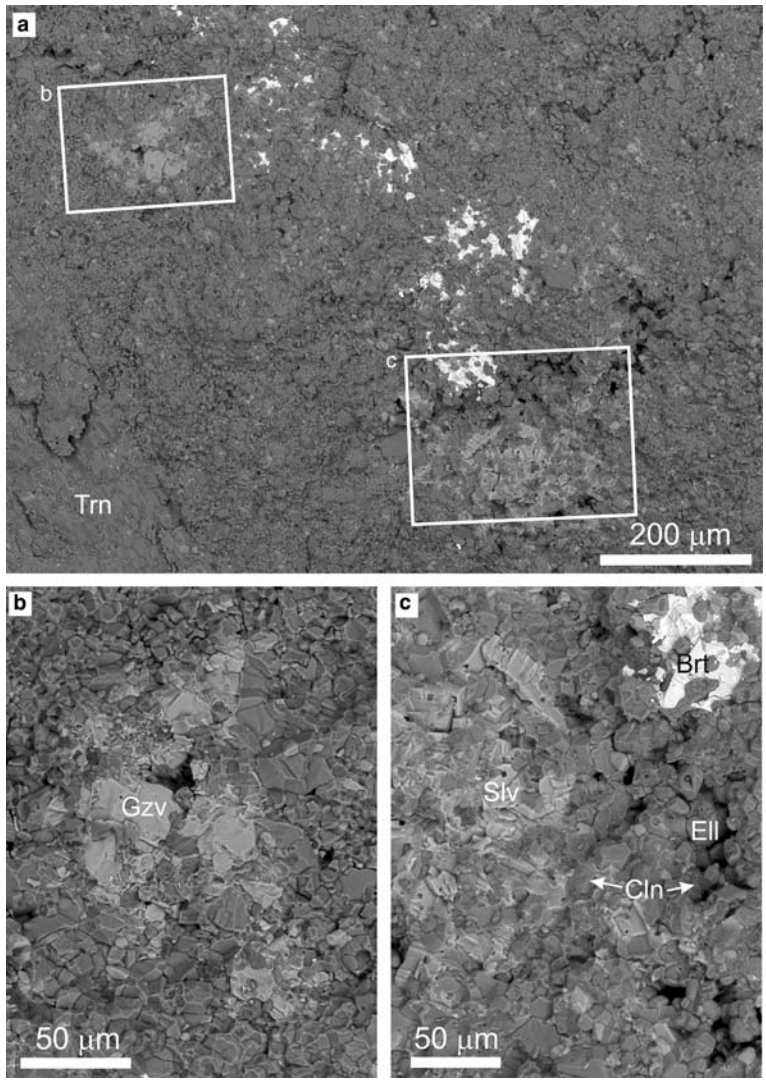

FIG. 3. Scanning electron microscopy BSE images using energy-dispersive spectroscopy in a low vacuum (40 Pa). Gazeevite (*a*, *b*) in specimen ZP4A accumulates within a porous, linear zone in larnite rock (fresh fracture); pores are partially filled with baryte, sylvite and calciolangbeinite (*a*, *c*). Gzv = gazeevite, Brt = baryte, Slv = sylvite, Cln = calciolangbeinite, Ell = fluorellestadite, Trn = ternesite

et al., 2015*a*). The crystal structure of eltyubyuite, $Ca_{12}Fe^{3+}_{10}Si_4O_{32}Cl_6$, was solved for a crystal from the Shadil-Khokh xenolith, Southern Ossetia (Gfeller *et al.*, 2015*c*).

Physical and optical properties

Gazeevite from all localities is colourless, transparent, with white streak and vitreous lustre; it does not show UV luminescence. Gazeevite is brittle, shows pronounced parting and imperfect cleavage along (001), and is uniaxial (–), $\omega = 1.640(3)$, $\varepsilon = 1.636(2)$ (for gazeevite from specimen DR5D, $\lambda = 589$ nm) and nonpleochroic; Mohs hardness ≈ 4.5; VHN load 50 g, range 353–473, mean (of 12) 417 kg mm^{-2} (specimen ZP4A). The density of gazeevite could not be measured because of abundant, tiny inclusions of ye'elmite, brownmillerite and larnite; the calculated density is 3.39 g cm^{-3} (specimen JBB11a) based on

https://doi.org/10.1180/minmag.2016.080.105 Published online by Cambridge University Press

TABLE 2. Chemical composition of gazeevite from Jabel Harmun (JBB11a, JB8, 14-3-6) and Nahal Darga (DR5D), Palestine Autonomy, Har Parsa, Negev Desert (ZP4A), Israel, Shadil-Khokh, Sothern Ossetia (U11).

	JBB11a			U11			ZP4A		
	Σ14	s.d.	range	Σ16	s.d.	range	Σ13	s.d.	range
SO_3	19.49	0.33	18.80–19.92	20.77	0.48	20.02–21.63	17.69	0.62	16.55–18.61
V_2O_5									
P_2O_5	2.70	0.52	1.60–3.51	0.09	0.07	0–0.23	2.99	0.20	2.62–3.35
TiO_2	0.09	0.04	0.03–0.21						
SiO_2	14.35	0.39	13.51–15.03	15.87	0.16	15.64–16.15	15.98	0.54	15.26–17.18
Al_2O_3	0.28	0.23	0.14–1.07	0.04	0.02	0–0.08	0.07	0.02	0.02–0.11
BaO	17.20	0.77	16.02–18.26	16.49	0.73	15.29–17.48	17.19	0.41	16.26–17.78
SrO	0.22	0.10	0.06–0.39	0.99	0.25	0.59–1.36			
CaO	44.09	0.19	43.90–44.65	44.04	0.33	43.62–44.77	44.25	0.34	43.91–45.16
K_2O	0.76	0.10	0.57–0.93	0.73	0.13	0.50–0.93	0.89	0.09	0.74–1.06
Na_2O	0.09	0.03	0.05–0.15	0.05	0.01	0.03–0.07	0.11	0.03	0.05–0.14
F	0.28	0.06	0.22–0.42	0.23	0.08	0.12–0.40	1.03	0.21	0.48–1.19
*–O = F	0.12			0.10			0.43		
Total	99.43			99.20			99.77		
Calculated on 17(O + F)									
Ba	0.854			0.821			0.850		
K	0.123			0.118			0.143		
Sr	0.016			0.073					
Sum A	0.993			1.012			0.993		
Ca	5.986			5.992			5.984		
Na	0.022			0.012			0.027		
Sum B	6.008			6.004			6.011		
Si	1.818			2.015			2.017		
Al	0.042			0.006			0.010		
Ti^{4+}	0.009								
P^{5+}	0.133								
Sum T1	2.002			2.021			2.027		
S^{6+}	1.853			1.979			1.676		
V^{5+}							0.000		
P^{5+}	0.147			0.010			0.319		
Sum T2	2.000			1.989			1.995		
F	0.112			0.092			0.411		
O	0.841			0.865			0.499		
Sum W	0.953			0.957			0.910		

(Continued)

the empirical formula and single-crystal X-ray diffraction (SCXRD) cell parameters.

Raman spectroscopy

Raman spectra of gazeevite were recorded using a WITec alpha300 R confocal Raman microscope (Institute of Physics, University of Silesia, Poland) equipped with a Nd:YAG laser (532 nm at 50 mW power on the sample), and a high sensitivity, back-illuminated Newton CCD camera captured the spectra. The excitation laser radiation was coupled into the microscope through a single-mode optical fibre with a diameter of 50 μm. An air Olympus MPLAN (100×/0.90NA) objective was used. Raman

https://doi.org/10.1180/minmag.2016.080.105 Published online by Cambridge University Press

TABLE 2. Continued.

	DR5D			JB8			14-3-6
	Σ13	s.d.	range	Σ8	s.d.	range	
SO_3	20.17	0.23	19.69–20.49	16.23	0.86	14.78–17.57	21.73
V_2O_5				0.30	0.07	0.22–0.44	0.00
P_2O_5	2.11	0.38	1.67–2.80	7.60	0.43	6.77–8.38	0.51
TiO_2	0.06	0.02	0.03–0.08	0.22	0.10	0.04–0.42	0.00
SiO_2	14.60	0.20	14.19–14.86	12.26	0.28	11.94–12.62	16.07
Al_2O_3	0.32	0.11	0.17–0.53	0.16	0.04	0.1–0.22	0.21
BaO	16.33	0.53	15.20–17.15	17.80	1.65	17.09–18.19	13.01
SrO	0.24	0.07	0.15–0.38	0.21	0.03	0.16–0.26	0.00
CaO	44.66	0.35	44.23–45.37	43.58	0.55	43.79–44.76	45.33
K_2O	1.05	0.12	0.93–1.35	0.68	0.07	0.56–0.81	2.65
Na_2O	0.09	0.03	0.02–0.11	0.14	0.07	0–0.24	0.16
F	0.41	0.06	0.31–0.53	0.35	0.11	0.24–0.55	1.08
*–O=F	0.17			0.15			0.45
Total	99.87			99.38			100.30
Calculated on 17(O+F)							
Ba	0.802			0.889			0.620
K	0.168			0.111			0.411
Sr	0.017			0.016			
Sum A	0.987			1.016			1.032
Ca	5.999			5.948			5.909
Na	0.022			0.035			0.038
Sum B	6.021			5.983			5.947
Si	1.830			1.562			1.955
Al	0.047			0.024			0.030
Ti^{4+}	0.006			0.021			
P^{5+}	0.123			0.396			0.036
Sum T1	2.006			2.003			2.021
S^{6+}	1.898			1.551			1.984
V^{5+}				0.025			
P^{5+}	0.101			0.424			0.017
Sum T2	1.999			2.000			2.001
F	0.163			0.141			0.416
O	0.818			0.846			0.498
Sum W	0.981			0.987			0.914

scattered light was focused onto a multi-mode fibre (50 μm diameter) and monochromator with a 600 mm^{-1} grating. Single Raman spectra were accumulated by five scans with integration time of 10–15 s and a resolution of 3 cm^{-1}. The spectrometer monochromator was calibrated using the Raman scattering line of a silicon plate (520.7 cm^{-1}).

The following main bands in the Raman spectra of gazeevite were observed (cm^{-1}): 160, 213, 266 and 315 (lattice mode, O–Ba–O and O–Ca–O vibration); 413 [$\nu_2(SiO_4)^{4-}$]; 468 [$\nu_2(SO_4)^{2-}$]; 529 [$\nu_4(SiO_4^{4-})$]; 638 [$\nu_4(SO_4^{2-})$]; 870 [$\nu_1(SiO_4^{4-})$; 1000 [$\nu_1(SO_4^{2-})$]; 1099 and 1135 [$\nu_3(SO_4^{2-})$] (Fig. 4). In Raman spectra of P-bearing gazeevite from the Hatrurim Complex additional bands at 963 cm^{-1} [$\nu_1(PO_4)^{4-}$] and 560 cm^{-1} [$\nu_4(PO_4)^{4-}$] appear, which are absent in the Raman spectra of gazeevite from Ossetia. Raman spectra of gazeevite are close to

https://doi.org/10.1180/minmag.2016.080.105 Published online by Cambridge University Press

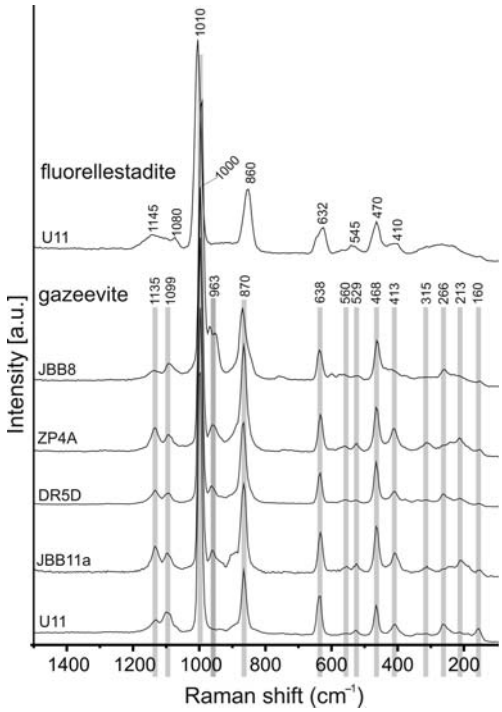

FIG. 4. Raman spectra of gazeevite from Jabel Harmun (JBB11a, JB8), West Parsa (ZP4A), Nahal Darga (DR5D), Shadil Khokh (U11), and chlorine-bearing fluorellestadite (U11).

those of fluorellestadite, $Ca_5[(SiO_4)_{1.5}(SO_4)_{1.5}]F$ (Fig. 4), but are distinct from those of ellestadite by the position of the main bands $\nu_1(SiO_4)^{4-}$ at 870 cm^{-1} and 860 cm^{-1} and $\nu_1(SO_4)^{2-}$ at 1000 cm^{-1} and 1010 cm^{-1} (Fig. 4). Raman spectra of gazeevite are also similar to those of minerals of the nabimusaite–dargaite series. A distinctive feature is the absence of a doublet at ~860 cm^{-1} (Galuskin *et al.*, 2015*b*, Dulski *et al.*, 2015) in the latter.

Structure of gazeevite

Unit-cell parameters were refined with SCXRD data of sample U11 (Shadil-Khokh) obtained with a SuperNova Dual diffractometer (Mo*K*α, λ = 0.71073 Å; Institute of Physics, University of Silesia, Poland) at 100 K. Unit-cell parameters of P-bearing gazeevite from the Jabel Harmun are a = 7.1540(1), c = 25.1242(5) Å, V = 1113.58(3) Å^3, Z = 3, $R\bar{3}m$; they are slightly larger than those of P-free gazeevite from Shadil Khokh, a = 7.1247(9), c = 25.007(4) Å, V = 1099.3(2) Å^3, Z = 3.

TABLE 3. Crystal data refinement parameters for gazeevite.

Crystal data	
Ideal formula	$BaCa_6(SiO_4)_2(SO_4)_2O$ (No.26)
Space group	$R\bar{3}m$
Unit cell dimensions (Å)	a = 7.1540(1), c = 25.1242(5)
Volume (Å^3)	1113.58(3)
Z	3
Chemical formula	$(Ba_{0.81}K_{0.19})Ca_6(SiO_4)_2(SO_4)_2O$
Intensity measurement	
Crystal shape	prism
Crystal size (mm)	0.04 × 0.03 × 0.02
Diffractometer	APEX II SMART
X-ray radiation; power	Mo*K*α; 50 kV 30 mA
Monochromator; temperature	Graphite; 293 K
Detector-to-sample distance	5 cm
Measurement method	Phi and Omega scans
Radiation width	0.5°
Time per frame	20 s
Max. θ° range for data collection	30.49
Index ranges	$-10 \le h \le 10$; $-10 \le k \le 7$; $-35 \le l \le 34$
No. of measured reflections	6106
No. of unique reflections	466
No. of observed reflections ($I > 2\sigma(I)$)	437
Refinement of the structure	
No. of parameters used in refinement	36
R_{int}; R_σ	0.0676; 0.0210
$R1$, I > 2σ(I)	0.0303
$R1$ all Data	0.0332
$wR2$ on (F^2)	0.0636
Goof	1.287
Δρ min (e Å^{-3}); Δρ max (e Å^{-3})	–1.19 close to O5; 0.75 close to Ca1

The crystal structure was determined using data of gazeevite from Jabel Harmun, ~0.04 mm × 0.03 mm × 0.02 mm (Grain no.26, sample JBB11a, Tables 3–6,), using a Bruker APEX II SMART diffractometer (Mo*K*α, λ = 0.71073 Å; University of Bern, Switzerland). Diffraction data were collected with ω scans at different φ settings (φ-ω scan) and were processed using *SAINT* (Bruker, 1999). An empirical absorption correction using *SADABS* (Sheldrick, 1996) was applied. The structure was solved by direct methods with subsequent analyses of difference-Fourier maps. The structure was refined using *SHELX97* (Sheldrick, 2008) to

https://doi.org/10.1180/minmag.2016.080.105 Published online by Cambridge University Press

TABLE 4. Atom coordinates, U_{eq} (Å^2) values for gazeevite.

Site	Atom	*x*/*a*	*y*/*b*	*z*/*c*	U_{eq}	Occ.
Ba1	Ba	1/3	2/3	1/6	0.0172(2)	0.810(6)
	K					0.190(6)
Ca1	Ca	0.84426(7)	0.68853(13)	0.05827(3)	0.0133(2)	1
*T*1	Si	2/3	2/3	0.03430(8)	0.0072(4)	1
*T*2	S	2/3	1/3	0.15488(7)	0.0095(3)	1
O1	O	1/3	2/3	0.9691(2)	0.0165(11)	1
O2	O	0.2096(3)	0.7904(3)	0.05347(15)	0.0237(8)	1
O3	O	0.6036(9)	0.1159(13)	0.1360(3)	0.0139(11)	0.405(3)
O3A	O	0.554(2)	0.108(4)	0.1309(11)	0.0139(11)	0.190(6)
O4	O	2/3	1/3	0.2143(2)	0.0144(11)	1
O5	O	0	0	0	0.0134(15)	1

TABLE 5. Anisotropic displacement parameters U^{ij} for gazeevite.

Site	U^{11}	U^{22}	U^{33}	U^{23}	U^{13}	U^{12}
Ba1	0.0175(3)	0.0175(3)	0.0166(4)	0.000	0.000	0.00874(14)
Ca1	0.0111(3)	0.0095(4)	0.0186(4)	0.0005(3)	0.00025(16)	0.00477(19)
*T*1	0.0060(5)	0.0060(5)	0.0096(9)	0.000	0.000	0.0030(2)
*T*2	0.0103(5)	0.0103(5)	0.0077(7)	0.000	0.000	0.0052(2)
O1	0.0187(17)	0.0187(17)	0.012(3)	0.000	0.000	0.0093(8)
O2	0.0157(11)	0.0157(11)	0.043(2)	–0.0053(7)	0.0053(7)	0.0107(13)
O4	0.0183(16)	0.0183(16)	0.007(2)	0.000	0.000	0.0091(8)
O5	0.016(2)	0.016(2)	0.009(3)	0.000	0.000	0.0079(11)

TABLE 6. Selected interatomic distances (Å) for gazeevite.

Ba1	O3* 6×	2.906(8)
	O3A* 6×	2.88(3)
Ca1	O1	2.3054(18)
	O2 2×	2.339(2)
	O3* 2×	2.525(7)
	O3A* 2×	2.656(18)
	O4	2.461(3)
	O5	2.4222(8)
*T*1	O2 3×	1.607(3)
	O4	1.639(6)
*T*2	O3* 3×	1.465(8)
	O3A* 3×	1.52(3)
	O4	1.492(5)

*Either O3 or O3A is occupied.

$R1 = 3.03\%$. The refinement including anisotropic atom displacement parameters was carried out with neutral-atom scattering factors. Additional smeared intensities in reciprocal space slices indicated an intergrowth of several other crystalline phases. For the refinement only the diffraction characteristics of the major fraction were considered. The site occupancies for the split O3/O3A position in the final refinement were constrained to give an overall occupancy resulting in the required oxygen contribution of 6 atoms per formula unit.

Gazeevite is isostructural with zadovite and aradite (Galuskin *et al.*, 2015*a*). The characteristic feature of the structure type is the intercalation of antiperovskite-like $\{[X\mathrm{Ca}_6](T\mathrm{O}_4)_2\}$ and $\mathrm{Ba}(T\mathrm{O}_4)_2$ layers, where *X* refers to O^{2-} in gazeevite and F^- in zadovite and aradite (Fig. 5*a*–*c*, Galuskin *et al.*, 2015*a*). The structure consists of two tetrahedral sites located on the three-fold axis. *T*1 is placed in the antiperovskite layer at 1/3, 2/3, 0.034. The *T*1 site has three shorter bonds towards O2 and one

https://doi.org/10.1180/minmag.2016.080.105 Published online by Cambridge University Press

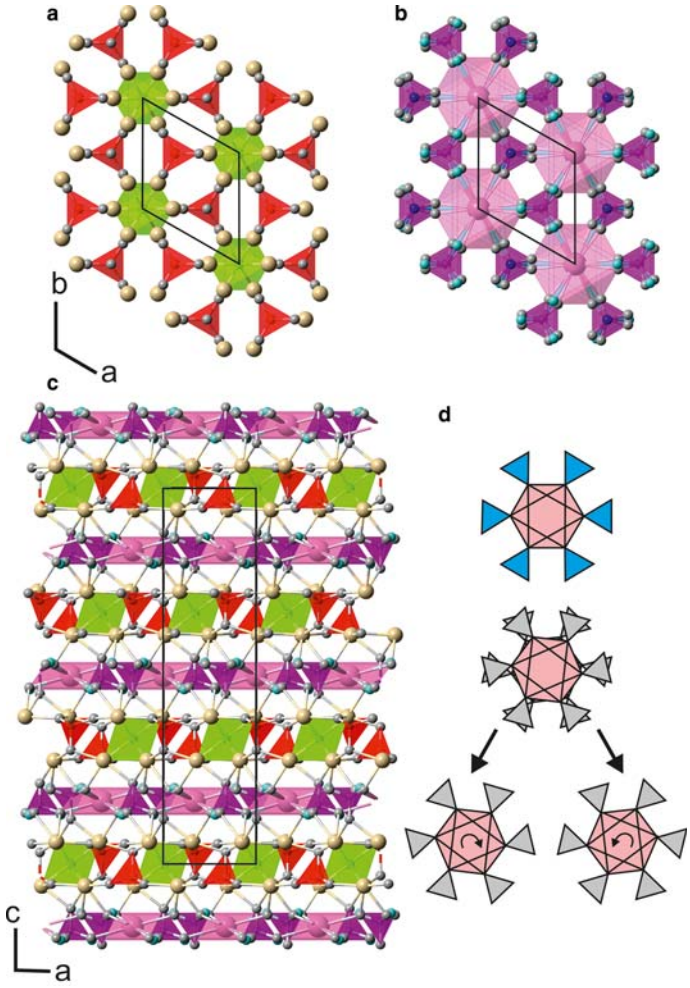

FIG. 5. The structure of $BaCa_6(SiO_4)_2(SO_4)_2O$ may be described as a 1:1 stacking of the two modules $\{[OCa_6](SiO_4)_2\}^{2+}$ (*a*) and $\{Ba(SO_4)_2\}^{2-}$ (*b*) along [001]. (*a*) Module consisting of Ca ions (yellow spheres) forming the corners of an octahedron (green), centred by O5. SiO_4 tetrahedra (red) fill gaps between the green OCa_6 octahedra. (*b*) Module characterized by (SO_4) tetrahedra (violet) connected to six-coordinate Ba (purple translucent octahedra). Oxygens are shown as grey spheres. The triangular bases of the tetrahedra display rotational disorder, indicated by partial occupation of the sites O3A (light blue) and O3 (grey). O4 (dark blue) indicates the apex of the tetrahedron. In (*c*) the stacking is shown in a projection along [010]. (*d*) Rotational disorder of the BaO_6 octahedron (pink) linked to six tetrahedra with the triangular base O3A–O3A–O3A (blue) and O3–O3–O3 (grey) is shown. The disorder of tetrahedra appears as a libration of ±6° around [001].

slightly longer bond along the rotation axis towards O1. In gazeevite the *T*1 site is occupied solely by Si, while in aradite and zadovite *T*1 has an overall charge of 4.5+ due to 1:1 occupancy of V/Si or P/Si, respectively (Galuskin *et al.*, 2015*a*). In gazeevite *T*2 is occupied by S^{6+} and bonds three times to O3 or O3A while the fourth apex (O4) along the three-fold axis is slightly longer, as observed for the *T*1 tetrahedron. *T*2, situated at 2/3, 1/3, 0.15 belongs to the intercalated $Ba(TO_4)_2$ module, which is characterized by a large cation site, usually occupied by Ba. The measured gazeevite single crystal shows a considerable amount of K (19.0(6)%) at this site.

The difference in ionic radius and charge of K compared to Ba causes splitting of the six

https://doi.org/10.1180/minmag.2016.080.105 Published online by Cambridge University Press

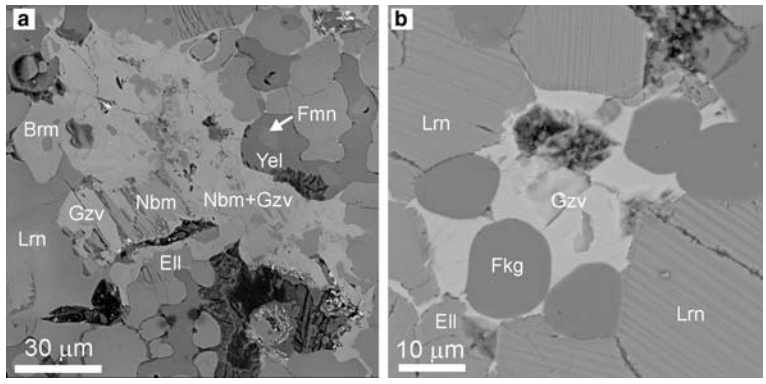

FIG. 6. (*a*) High-potassium gazeevite replacing nabimusaite. (*b*) High-phosphorus gazeevite in larnite rock, BSE. Gzv = gazeevite, Nbm = nabimusaite, Ell = fluorellestadite, Fmn = fluormayenite, Fkg = fluorkyuygenite, Lrn = larnite, Brm = brownmillerite, Yel = ye'elimite.

coordinating O3 sites. Therefore, O3 was split into two sub-sites, O3 and O3A, where O3 is connected to Ba [2.906(8) Å] and O3A to K [2.88(3) Å]. While O3A lies at a special position on a mirror plane as observed for zadovite and aradite, O3 is displaced 0.354(18) Å from O3A and resides at a general position (Fig. 5*c*). The doubled multiplicity of O3 relative to O3A implies two possible arrangements of the base triangle O3–O3–O3 of the *T*2 site. This effect is related to rotation of BaO_6 octahedra about the three-fold axis by ~6° (Fig. 5*d*) and an increase of Ba–O3 distances compared to Ba–O3A and a decrease of the *T*2–O3 distance (1.465(8) Å) compared to *T*2–O3A (1.52(3) Å, Table 6). The slightly enlarged tetrahedron coordinated by O3A may indicate partial P content as expected for $K(PO_4)_2^{5-}$ replacing the $Ba(SO_4)_2^{2-}$ module. The necessary charge balance is obtained by F^- at the O5 site and P^{5+} at *T*1. Due to similar scattering powers of P/Si and F/O, respectively, minor P and F have not been included in the structure refinement. However, the correctness of this substitution is confirmed by the electron microprobe analysis (EMPA) data, with $Ba_{0.81}K_{0.19}Ca_6(SiO_4)_2(SO_4)_2O_{0.81}F_{0.19}$ (SCXRD) and $(Ba_{0.85}K_{0.12}Sr_{0.02})_{\Sigma 0.99}(Ca_{5.99}Na_{0.02})_{\Sigma 6.01}[(SiO_4)_{1.82}(PO_4)_{0.14}(AlO_4)_{0.04}(TiO_4)_{0.01}]_{\Sigma 2.01}[(SO_4)_{1.85}(PO_4)_{0.15}]_{\Sigma 2}O_{0.84}F_{0.11}$ (EMPA, Table 2).

Because gazeevite occurs only in small concentrations and its crystals contain a large amount of other mineral inclusions, powder XRD data were not collected, but calculated more reliably from the results of the single-crystal structure refinement (Table S1; supplementary material deposited with the Principal Editor of *Mineralogical Magazine* and available from http://www.minersoc.org/pages/e_journals/dep_mat_mm.html).

Discussion

Gazeevite was found in two genetic types of pyrometamorphic rocks. In both cases gazeevite is a product of high-temperature alteration of early mineral associations of pyrometamorphic rocks having a high content of fluorellestadite and often oldhamite. Gazeevite is a common mineral of larnite rocks of the Hatrurim Complex crystallizing together with minerals of the nabimusaite–dargaite series. In xenoliths of the Shadil-Khokh volcano gazeevite is a very rare mineral. In both types of rocks gazeevite forms xenomorphic, poikilitic metacrysts and irregular aggregates substituting fluorellestadite and larnite. Water-soluble sulfates and chlorides in rocks of the Hatrurim Complex are, in our opinion, products of melt crystallization generated during the abating combustion process. Reaction of these melts (fluids) with early minerals of a typical 'clinker association', fluorellestadite, larnite, oldhamite and others, leads to crystallization of gazeevite, nabimusaite–dargaite and ternesite (Galuskin *et al.*, 2016). Probably, an intergranular sulfate-containing melt (fluid) in the rocks of the Shadil-Khokh volcano is responsible for gazeevite formation. Appearance of jasmundite in association with gazeevite may indicate that alteration of primary mineral associations proceeded not only with melt but also with gases.

In contrast to the altered xenoliths of Ossetia, gazeevite is a widespread mineral in larnite rocks of

https://doi.org/10.1180/minmag.2016.080.105 Published online by Cambridge University Press

the Hatrurrim Complex. Usually, it contains up to 3 wt.% PO_4 and ~1 wt.% K_2O as impurities. High-potassium gazeevite substituting nabimusaite (Fig. 6*a*; Table 2, sample 14-3-6) was detected. The maximum content of $KCa_6(SiO_4)_2(SO_4)_2F$ potential end-member is ~40%. In larnite rocks with primary high-phosphorus fluorellestadite, gazeevite contains 7.6 wt.% PO_4 (Fig. 6*b*, Table 2, sample JB8), leading to a chemical composition with 10% $KCa_6(SiO_4)_2(SO_4)_2F$ and 20% $BaCa_6(PO_4)_2$ $(PO_4)_2O$ potential end-members. It may also be assumed that phosphorus is combined with the potassium end-member; in that case the mineral contains 10% $KCa_6(PO_4)_2(PO_4)_2F$ and 10% $BaCa_6(PO_4)_2(PO_4)_2O$. The Raman spectrum of high-P gazeevite is distinct from other gazeevite spectra by the appearance of two bands related to $\nu_1(PO_4)^{4-}$ vibrations, suggesting high P content at both *T*1 and *T*2 corresponding to the isomorphic scheme: $(SiO_4)^{4-} + (SO_4)^{2-} \Leftrightarrow 2(PO_4)^{3-}$. Such isomorphism is characteristic for holotype gazeevite JBB11a and co-type DR5D (Table 2). In gazeevite from Har Parsa the isomorphic scheme $(SO_4)^{2-} + O^{2-} \Leftrightarrow (PO_4)^{3-} + F^-$ is only at *T*2, yielding the theoretical end-member $BaCa_6(SiO_4)_2[(PO_4)(SO_4)]F$. Isomorphous substitution according the scheme $(SO_4)^{2-} + O^{2-} \Rightarrow (PO_4)^{3-} + F^-$ suggests the occurrence of a potentially new P-analogue of dargaite with end-member formula $BaCa_{12}(SiO_4)_4(PO_4)_2F_2O$, belonging to the nabimusaite group, which was found in larnite and spurrite rocks of the Hatrurim Complex in Jordan and Israel (Galuskin *et al.*, 2015*d*). This type of isomorphic substitution allows us to suppose the existence of a P-analogue of nabimusaite with the end-member formula $KCa_{12}(SiO_4)_4(PO_4)_2F_3$.

Acknowledgements

The authors thank Peter Williams, Ritsuro Miyawaki, Peter Leverett and the anonymous reviewers for their careful reviews which helped to improve a previous version of the manuscript. Investigations were partially supported by the National Sciences Centre (NCN) of Poland by decision no. 2013/11/B/ST10/00272 (I.G. and E.G.).

References

Bentor, Y.K. (editor) (1960) *Lexique Stratigraphique International, Asie. Volume III, Section 10.2, Israel*. Centre National de la Research Scientifique, Paris.

Britvin, S.N., Murashko, M.N., Vapnik, Y., Polekhovsky, Y.S. and Krivovichev, S.V. (2015) Earth's phosphides in Levant and insights into the source of Archean prebiotic phosphorus. *Science Reports*, **5**, 8355.

Bruker (1999) *SMART and SAINT-Plus.* Versions 6.01. Bruker AXS Inc., Madison, Wisconsin, USA.

Dulski, M., Wrzalik, R., Galuskina, I. and Galuskin, E. (2015) Raman investigation of new and potentially new minerals of nabimusaite supergroup. *Periodico di Mineralogia*, ECMS 2015, 67–68.

Fayos, J., Glasser, F.P., Howie, R.A., Lachowski, E. and Perez-Mendez, M. (1985) Structure of dodecacalcium potassium fluoride dioxide terasilicate bis (sulphate), $KF{\cdot}2[Ca_6(SO_4)(SiO_4)_2O]$: a fluorine containing phase encountered in cement clinker production process. *Acta Crystallographica*, **C41**, 814–816.

Galuskin, E.V., Galuskina, I.O., Kusz, J. Armbruster, T., Marzec, K.M., Dzierżanowski, P. and Murashko, M. (2014) Vapnikite Ca_3UO_6 – a new double-perovskite mineral from pyrometamorphic larnite rocks of the Jabel Harmun, Palestinian Autonomy, Israel. *Mineralogical Magazine*, **78**, 571–581.

Galuskin, E.V., Gfeller, F., Galuskina, I.O., Pakhomova, A., Armbruster, T., Vapnik, Y., Włodyka, R., Dzierżanowski, P. and Murashko, M. (2015*a*) New minerals with modular structure derived from hatrurite from the pyrometamorphic Hatrurim Complex, Part II: Zadovite, $BaCa_6[(SiO_4)(PO_4)](PO_4)_2F$, and aradite, $BaCa_6[(SiO_4)(VO_4)](VO_4)_2F$, from paralavas of the Hatrurim Basin, Negev Desert, Israel. *Mineralogical Magazine*, **79**, 1073–1087.

Galuskin, E.V., Gfeller, F., Armbruster, T., Galuskina, I. O., Vapnik, Ye., Murashko, M., Wodyka, R. and Dzierżanowski, P. (2015*b*) New minerals with modular structure derived from hatrurite from the pyrometamorphic Hatrurim Complex, Part I: Nabimusaite, $KCa_{12}(SiO_4)_4(SO_4)_2O_2F$, from larnite rock of the Jabel Harmun, Palestinian Autonomy, Israel. *Mineralogical Magazine*, **79**, 1061–1072.

Galuskin, E.V., Gfeller, F., Armbruster, T., Galuskina, I. O., Vapnik, Y., Dulski, M., Murashko, M., Dzierżanowski, P., Sharygin, V.V., Krivovichev, S.V. and Wirth, R. (2015*c*) Mayenite supergroup, Part III: Fluormayenite, $Ca_{12}Al_{14}O_{32}$ $[\square_4F_2]$, and fluorkyuygenite, $Ca_{12}Al_{14}O_{32}[(H_2O)_4F_2]$, two new minerals of mayenite supergroup from pyrometamorphic rock of Hatrurim Complex. *European Journal of Mineralogy*, **27**, 123–136.

Galuskin, E.V., Gfeller, F., Galuskina, I.O., Armbruster, T. M., Vapnik, Y., Murashko, M.N. and Gazeev, V.M. (2015*d*) New and potentially new minerals of nabimusaite family with modular antiperovskite structures. *Abstracts of XII General Meeting of the Russian Mineralogical Society*, 302–304.

Galuskin, E.V., Galuskina, I.O., Gfeller, F., Krüger, B., Kusz, J., Vapnik, J., Dulski, M. and Piotr Dżierzanowski,

https://doi.org/10.1180/minmag.2016.080.105 Published online by Cambridge University Press

P. (2016) Silicocarnotite, $Ca_5[(SiO_4)(PO_4)](PO_4)$, a new 'old' mineral from the Negev Desert, Israel, and the ternesite–silicocarnotite solid solution: indicators of high-temperature alteration of pyrometamorphic rocks of the Hatrurim Complex, Southern Levant. *European Journal of Mineralogy*, **28**, 105–123.

Galuskina, I.O., Vapnik, Y., Prusik, K., Dzierżanowski, P., Murashko, M., Galuskin, E.V. (2013) Gurimite, IMA 58 2013–032. CNMNC Newsletter No. 16, August 2013, page 2708. *Mineralogical Magazine*, **77**, 2695–2709.

Galuskina, I.O., Vapnik, Ye., Lazic, B., Armbruster, T., Murashko, M. and Galuskin, E.V. (2014*a*) Harmunite $CaFe_2O_4$ – a new mineral from the Jabel Harmun, West Bank, Palestinian Autonomy, Israel. *American Mineralogist*, **99**, 965–975.

Galuskina, I.O., Vapnik, Y., Lazic, B., Armbruster, T., Murashko, M. and Galuskin, E.V. (2014*b*) Dzierżanowskite, IMA 2014-032. CNMNC Newsletter No. 21, August 2014, page 802; *Mineralogical Magazine*, **78**, 797–804.

Galuskina, I.O., Galuskin, E.V., Pakhomova, A.S., Widmer, R., Armbruster, T., Lazic, B., Grew, E.S., Vapnik, Y., Dzierżanowski, P. and Murashko, M. (2014*c*) Khesinite, IMA2014–033. CNMNC Newsletter No. 21, August 2014, page 838; *Mineralogical Magazine*, **78**, 833–840.

Galuskina, I.O., Krüger, B., Galuskin, E.V., Armbruster, T., Gazeev, V.M., Włodyka, R., Dulski, M. and Piotr Dzierżanowski (2015*a*) Fluorchegemite, $Ca_7(SiO_4)_3F_2$, a new mineral from the edgrewite-bearing endoskarn zone of an altered xenolith in ignimbrites from upper Chegem caldera, northern Caucasus, Kabardino-Balkaria, Russia: occurrence, crystal structure, and new data on the mineral assemblages. *The Canadian Mineralogist*, **53**, 325–344.

Galuskina, I.O., Galuskin, E.V., Prusik, K., Vapnik, Y., Dzierżanowski, P. and Murashko, M. (2015*b*) Hexacelsian, IMA2015-045. CNMNC Newsletter No. 27, October 2015, page 1224; *Mineralogical Magazine*, **79**, 1229–1236.

Gazeev, V.M., Zadov, A.E., Gurbanov, A.G., Pertsev, N. N., Mokhov, A.V. and Dokuchaev, A.Y. (2006) Rare minerals from Verkhniechegemskaya caldera (in xenoliths of skarned limestone). *Vestnik Vladikavkazskogo Nauchnogo Centra*, **6**, 18–27.

Gazeev, V.M., Gurbanova, O.A., Zadov, A.E., Gurbanov, A.G., Leksin, A.B. (2012) Mineralogy of skarned carbonate xenoliths from Shadil-Khokh volcano (Kelski volcanic area of the Great Caucasian Range). *Vestnik Vladikavkazskogo Nauchnogo Centra*, **2**, 23–33 [in Russian].

Gfeller, F., Galuskin, E.V., Galuskina, I.O., Armbruster, T., Vapnik, Ye., Włodyka, R. and Dzierżanowski, P. (2013) Natural $BaCa_6[(SiO_4)(PO_4)](PO_4)_2F$ with a new modular structure type. Goldschmidt 2013 Conference Abstracts, *Mineralogical Magazine*, **77**, 1160; https://doi.org/10.1180/minmag.2013.077.5.7

Gfeller, F., Galuskina, I.O., Galuskin, E.V., Armbruster, T., Vapnik, Y., Dulski, M., Gardocki, M., Jeżak, L. and Murashko, M. (2015*a*) Dargaite, IMA 2015-068. CNMNC Newsletter No. 28, December 2015, page 1860; *Mineralogical Magazine*, **79**, 1859–1864.

Gfeller, F., Widmer, R., Galuskin, E.V., Galuskina, I.O. and Armbruster, T. (2015*b*) The crystal structure of flamite and its relation to Ca_2SiO_4 polymorphs and nagelschmidtite. *European Journal Mineralogy*, **27**, 755–769.

Gfeller, F., Środek, D., Kusz, J., Dulski, M., Gazeev, V., Galuskina, I., Galuskin, E. and Armbruster, T. (2015*c*) Mayenite supergroup, part IV: Crystal structure and Raman investigation of Al-free eltyubyuite from the Shadil-Khokh volcano, Kel' Plateau, Southern Ossetia. *European Journal Mineralogy*, **27**, 137–143.

Gross, S. (1977) The mineralogy of the Hatrurim Formation, Israel. *Geological Survey of Israel Bulletin*, **70**, 1–80.

Jeffery, J.W. (1952) The crystal structure of tricalcium silicate. *Acta Crystallographica*, **5**, 26–35.

Krivovichev, S.V. (2008) Minerals with antiperovskite structure: a review. *Zeitschrift für Kristallographie*, **223**, 109–113.

Krüger, H. (2010) $Ca_{5.45}Li_{3.55}[SiO_4]_3O_{0.45}F_{1.55}$ and $Ca_7K[SiO_4]_3F_3$: single-crystal synthesis and structures of two trigonal oxyfluorides. *Zeitschrift für Kristallographie*, **225**, 418–424.

Mumme, W.G. (1995) Crystal structure of tricalcium silicate from a portland cement clinker and its application to quantitative XRD analysis. *Neues Jahrbuch für Mineralogie Monatshefte*, **1995**, 145–160.

Murashko, M.N., Chukanov, N.V., Mukhanova, A.A., Vapnik, Y., Britvin, S.N., Polekhovsky, Y.S. and Ivakin, Y.D. (2011) Barioferrite $BaFe_{12}O_{19}$: A new mineral species of the magnetoplumbite group from the Hatrurim Formation in Israel. *Geology Ore Deposit*, **7**, 558–563.

Nishi, F. and Takéuchi, Y. (1984) The rhombohedral structure of tricalcium silicate at 1200°C. *Zeitschrift für Kristallographie*, **168**, 197–212.

Sharygin, V.V., Lazic, B., Armbruster, T.M., Murashko, M.N., Wirth, R., Galuskina, I.O., Galuskin, E.V., Vapnik, Y., Britvin, S.N. and Logvinova, A.M. (2013) Shulamitite $Ca_3TiFe^{3+}AlO_8$ – A new perovskite-related mineral from Hatrurim Basin, Israel. *European Journal Mineralogy*, **25**, 97–111.

Sheldrick, G.M. (1996) *SADABS*. University of Göttingen, Germany.

Sheldrick, G.M. (2008) A short history of SHELX. *Acta Crystallographica*, **A64**, 112–122.

Sokol, E.V., Seryotkin, Y.V., Kokh, S.N., Vapnik, Y., Nigmatulina, E.N., Goryainov, S.V., Belogub, E.V. and Sharygin, V.V. (2015) Flamite, $(Ca,Na,K)_2(Si,P)O_4$, a

new mineral from ultrahigh-temperature combustion metamorphic rocks, Hatrurim Basin, Negev Desert, Israel. *Mineralogical Magazine*, **79**, 583–596.

Sokolova, E.V., Yamnova, N.A., Egorov-Tismenko, Y.K. and Khomyakov, A.P. (1984) The crystal structure of a new sodium-calcium-barium phosphate of Na, Ca and Ba $(Na_5Ca)Ca_6Ba(PO_4)_6F_3$. *Doklady Akademii Nauk SSSR*, **274**, 78–83.

Vapnik, Y., Sharygin, V.V., Sokol, E.V. and Shagam, R. (2007) Paralavas in a combustion metamorphic complex: Hatrurim Basin, Israel. *Reviews in Engineering Geology*, **18**, 1–21.

https://doi.org/10.1180/minmag.2016.080.105 Published online by Cambridge University Press